Supplement of Biogeosciences, 15, 6997–7024, 2018
https://doi.org/10.5194/bg-15-6997-2018-supplement

Biogeosciences Open Access EGU

Supplement of

Factors controlling coccolithophore biogeography in the Southern Ocean

Cara Nissen et al.

Correspondence to: Cara Nissen (cara.nissen@usys.ethz.ch)

The supporting information provides additional information about data sets used for model evaluation (section S1), as well as additional figures (section S2), with respect to model validation (Fig. S1-S4), factors controlling differences in light limitation between coccolithophores and diatoms (Fig. S5), the interplay of coccolithophores and small phytoplankton (Fig. S6-S7), the results of the sensitivity simulations (Fig. S8-S9), functional responses for phytoplankton growth and grazing in BEC (S10), simulated total chlorophyll seasonality (S11), and simulated carbon-to-chlorophyll ratios of coccolithophores and diatoms (S12).

S1: Data for model evaluation

Data used to validate physical and biogeochemical variables relevant for phytoplankton growth are presented in Table A1 in the main text. To assess the model's performance in simulating phytoplankton biogeography, community structure and pheonology, we compare model results to existing observations. We validate ROMS-BEC with biomass observations for diatoms (Leblanc et al., 2012) and coccolithophores (O'Brien et al., 2013) from the MAREDAT initiative. We combined the MAREDAT data set with recently published abundance data of coccolithophores (Balch et al., 2016; Saavedra-Pellitero et al., 2014; Tyrrell and Charalampopoulou, 2009; Gravalosa et al., 2008; Cubillos et al., 2007) and diatoms (Balch et al., 2016), thereby increasing the number of available data points threefold. New cell count data were converted to biomass estimates following the MAREDAT protocol (O'Brien et al., 2013; Leblanc et al., 2012). Based on available information in the literature, each species is first assigned an idealized shape (e.g. sphere for *E. huxleyi*), as well as a mean size (e.g. mean coccosphere diameter for *E. huxleyi*). Assuming the cytoplasm diameter to be 60% of the coccosphere diameter, we then calculate the mean biovolume of each cell. To get estimates of carbon biomass for each cell, the biovolume is ultimately multiplied with the specific carbon conversion factors from Menden-Deuer and Lessard (2000). The uncertainty range of this conversion is obtained by repeating the conversion using the minimum and maximum reported diameter for each species, respectively, and reporting the uncertainty range in percent of the mean biomass estimate. If no species information was provided, cell dimensions and carbon content for *E. huxleyi* and *F. pseudonana* were used in the conversion, as these two species appear to dominate the SO coccolithophore (e.g. Smith et al., 2017; Saavedra-Pellitero et al., 2014; Gravalosa et al., 2008) and diatom community (Smith et al., 2017), respectively. Since *F. pseudonana* is a rather small diatom (nanophytoplankton) and diatom biomass conversion factors in the MAREDAT database span about three orders of magnitude, we acknowledge that the resulting diatom biomass estimates are possibly lower bounds.

To obtain information about the relative contributions of the individual phytoplankton types to total phytoplankton biomass, we use the CHEMTAX climatology based on high performance liquid tomography (HPLC) data compiled by Swan et al. (2016). While the allocation of one specific pigment type to a model PFT is difficult (e.g. for HAPTO-6 and coccolithophores, see Swan et al., 2016), we use the data to identify spatial patterns of phytoplankton community composition (e.g. the change in the relative contribution of diatoms and coccolithophores to total phytoplankton biomass between high and low southern hemisphere latitudes) and compare them to patterns simulated with ROMS-BEC.

Bloom metrics are used to assess phytoplankton phenology in ROMS-BEC. We define the bloom start as the day when the respective PFT biomass concentration first surpasses 5% above its annual median (bloom threshold, July-June) for a minimum of 14 consecutive days (Soppa et al., 2016). The day of the bloom peak is reached at maximum PFT biomass concentration after the bloom start. The bloom end is then defined as the first day after the bloom peak when PFT biomass concentration falls

below the bloom threshold for a minimum of 14 consecutive days. To capture bloom initiation at high SO latitudes, a year runs from 1 July to 30 June.

To evaluate simulated coccolithophore calcification rates in ROMS-BEC, we use monthly binned particulate inorganic carbon [mg PIC m^{-3}], chlorophyll [mg chl m^{-3}] and SST [°C] climatologies from MODIS Aqua (NASA-OBPG, 2014b,a,c) to derive calcification rates C [mg PIC m^{-3} d^{-1}] following Eq. 1 in Balch et al. (2007):

$$\begin{aligned} \mathrm{C} = (&-0.0063 \cdot \mathrm{Z} + 0.05081 \cdot \mathrm{PIC} - 0.01055 \cdot \mathrm{Chl} \\ &+ 0.05806 \cdot \mathrm{D} - 0.0079 \cdot \mathrm{SST} - 0.4008)/0.2694 \end{aligned} \tag{1}$$

Z denotes the depth (here, we set $Z = 1$) and D is the daylength in hours, here calculated for the 15th of each month. The calcification rates are then integrated over the euphotic depth Z_{eu} using the satellite-derived chlorophyll concentrations (see Eq. 2 in Balch et al., 2007):

$$\mathrm{Z_{eu}} = 38 \cdot \mathrm{Chl}^{-0.428} \tag{2}$$

In the main text, we give a short overview of the model evaluation of relevant physical and biogeochemical properties (e.g. SST, MLD, nutrients) in section 4.1 and focus the model evaluation on the spatial and temporal variability of SO phytoplankton community structure in sections 4.2-4.4. Supplementary figures from the model evaluation can be found in this document (Fig. S1-S4).

S2: Additional figures

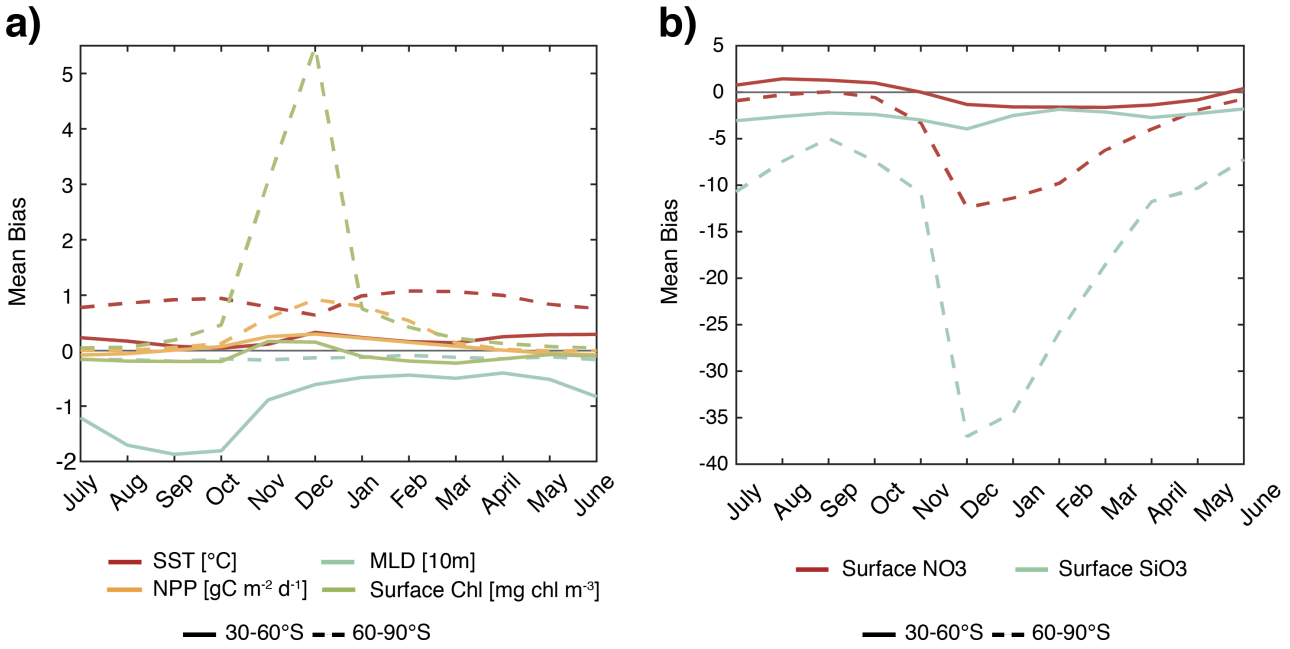

Figure S1: Temporal evolution of the model bias (reference simulation - observations). Shown are the average bias between 30-60°S (solid) and 60-90°S (dashed) for a) sea surface temperature (SST, red, [°C]), mixed layer depth (MLD, blue, [m]), net primary production (NPP, yellow, [gC m^{-2} d^{-1}]) and total surface chlorophyll (Chl, green, [mg chl m^{-3}]) and b) surface nitrate (NO3, red, [mmol m^{-3}]) and surface silicate (SiO3, blue, [mmol m^{-3}]). See Table A1 in the main text for data sources.

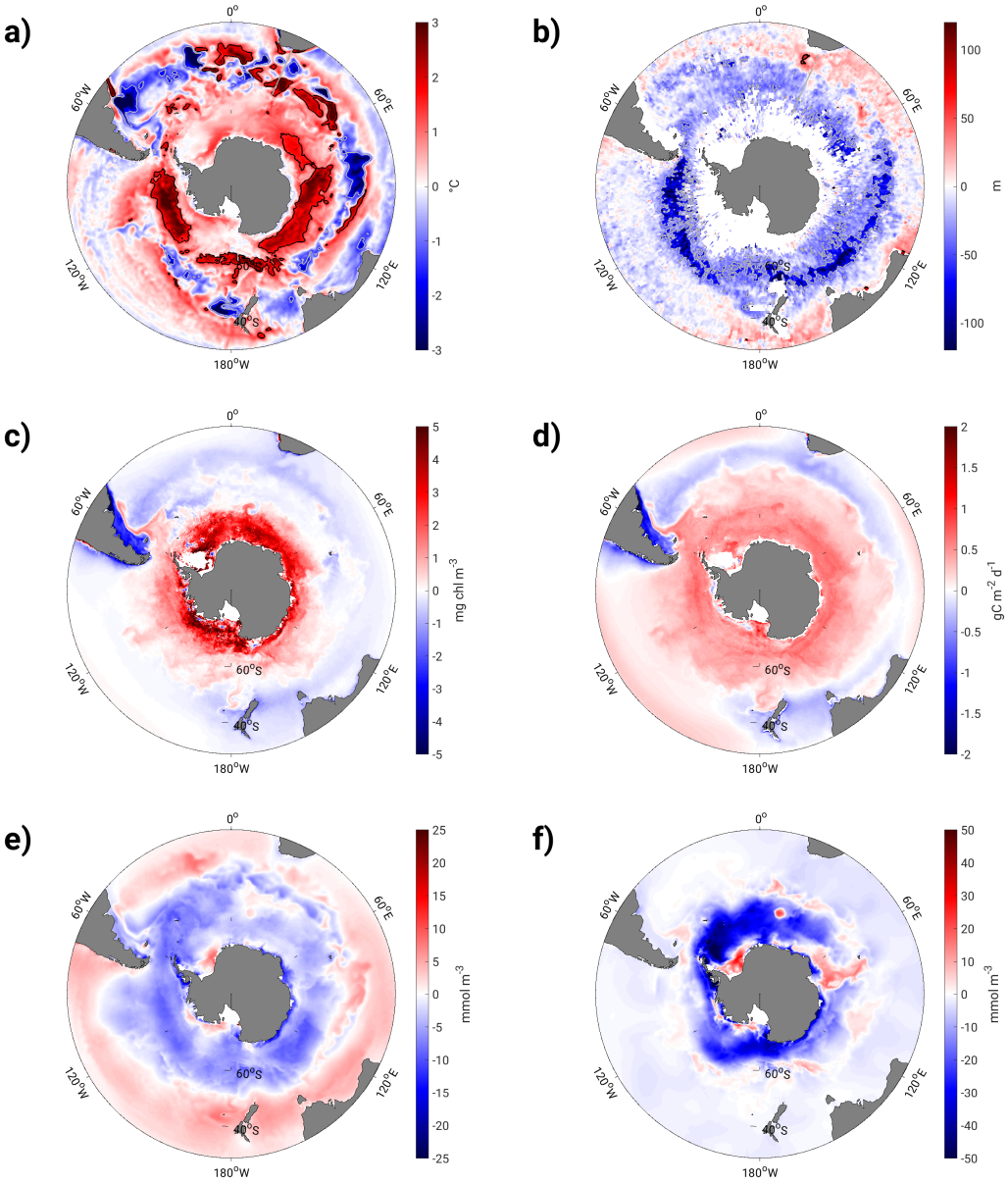

Figure S2: Annual mean bias of a) sea surface temperature [°C], b) mixed layer depth [m] , c) surface total chlorophyll [mg chl m^{-3}], d) net primary productivity [gC m^{-2} d^{-1}], e) surface nitrate [mmol m^{-3}], and f) surface silicate [mmol m^{-3}]. A positive bias denotes an overestimation in the model. See Table A1 in the main text for data sources.

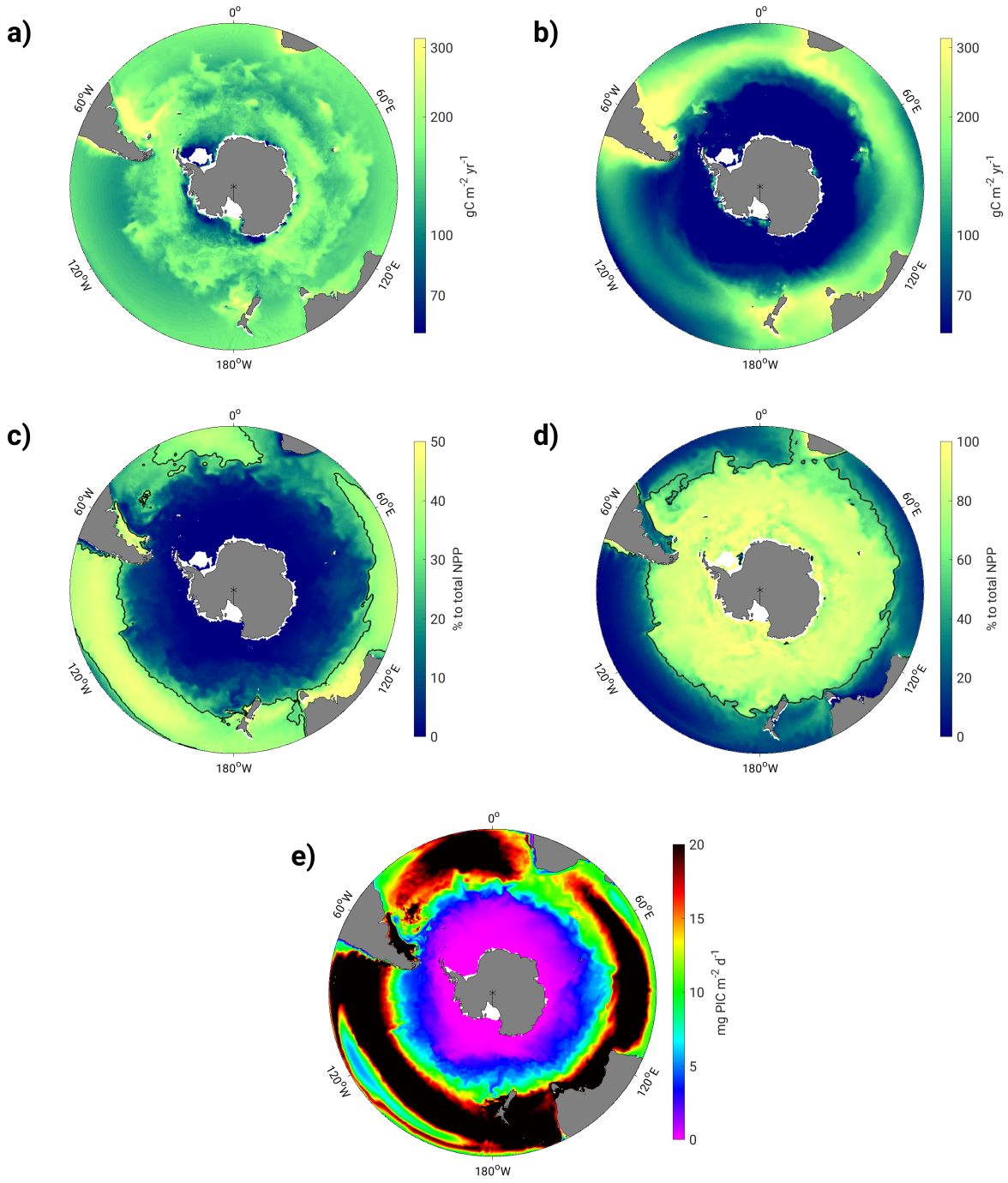

Figure S3: Total annually and vertically integrated NPP [gC m^{-2} yr^{-1}] in a) ROMS-BEC and b) in the MODIS Aqua VGPM climatology (Behrenfeld and Falkowski, 1997; O'Malley, 2016). Contribution [%] of c) coccolithophores and d) diatoms to total annually and vertically integrated NPP in ROMS-BEC. e) Annual mean calcification rates [mg PIC m^{-2} d^{-1}] by coccolithophores in ROMS-BEC.

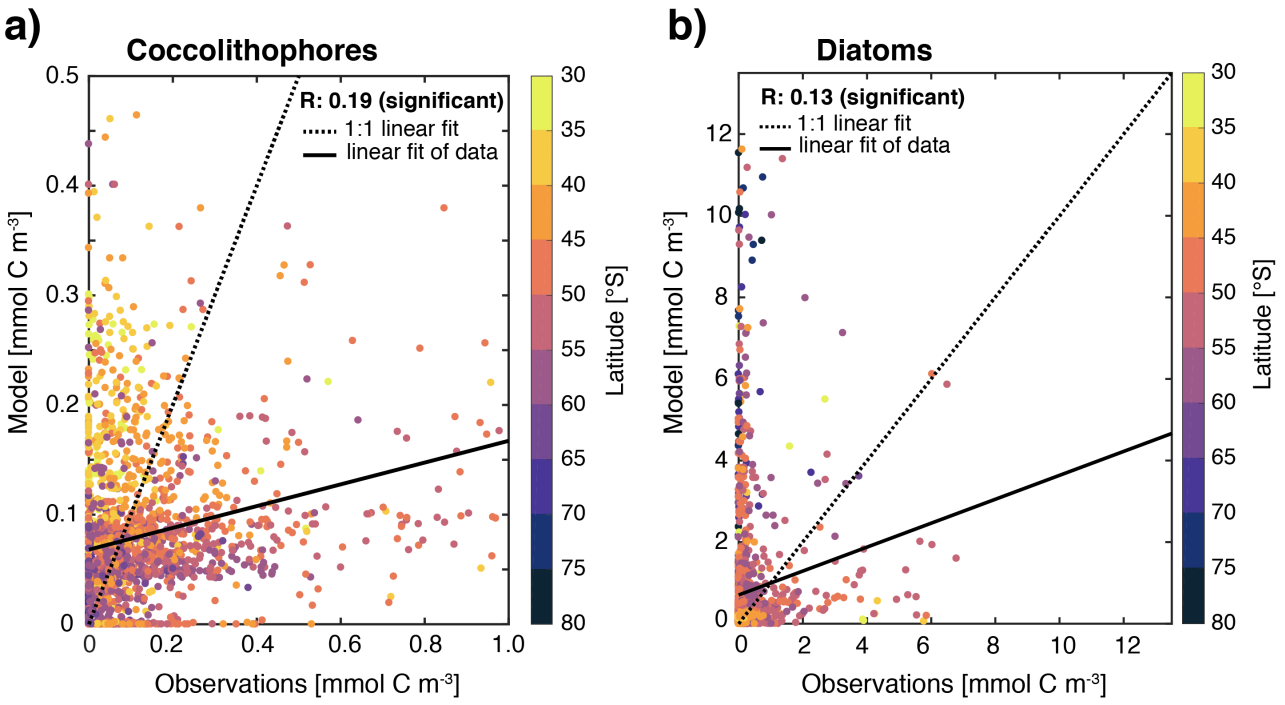

Figure S4: Validation of a) coccolithophore and b) diatom biomass [mmol C m^{-3}]. Model output is colocated with observations in space and time, observational data from all months and from above 1000m are considered here. See Table A1 in the main text for data sources. Dotted line shows the perfect linear 1:1 fit, whereas the solid line is the actual fit of the data (linear regression). Pearson correlation coefficients of these regressions are given in the top right, both are statistically significant ($p<0.05$). Points are color-coded according to the sampling latitude.

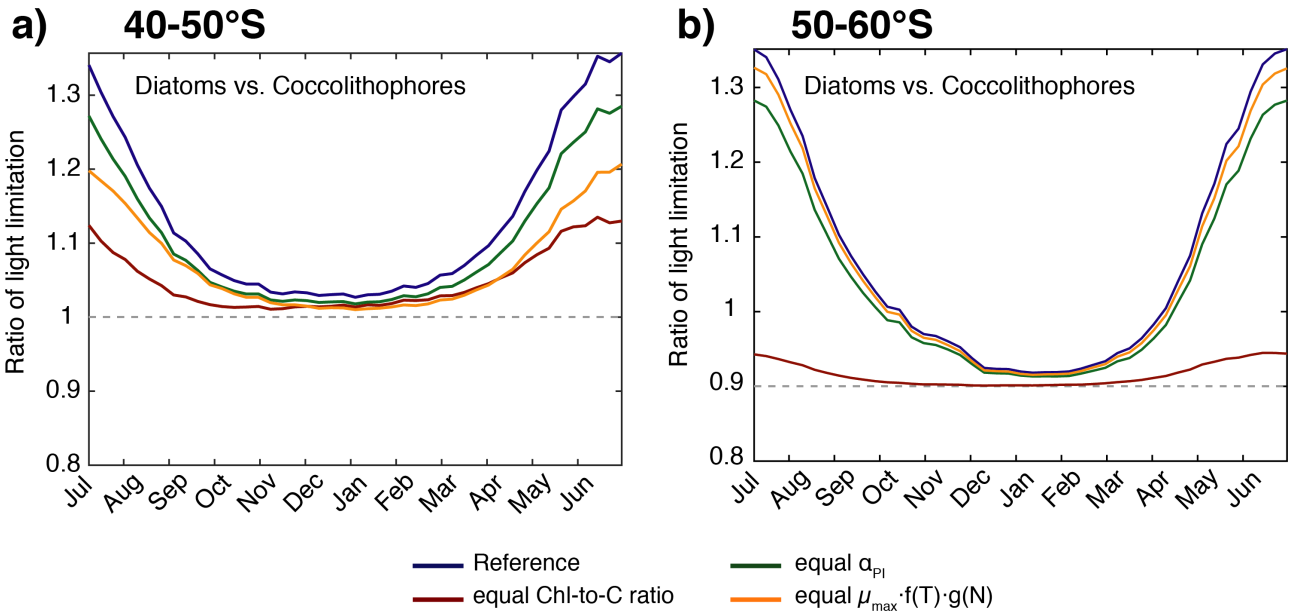

Figure S5: Assessing the controls on differences in light limitation between diatoms and coccolithophores for a) 40-50°S and b) 50-60°S. If the plotted ratio is equal one, there is no differences in light limitation between diatoms and coccolithophores. The reference run is shown in blue. We consecutively replaced the three possible controls (chlorophyll-to-carbon ratio in red, α_{PI} in green, $\mu_{\max} \cdot \mathrm{f(T)} \cdot \mathrm{g(N)}$ in yellow, see also Eq. B9 in main manuscript) in the calculation of light limitation for coccolithophores by the respective field of diatoms. For both latitudinal bands, differences in the chlorophyll-to-carbon ratio have the largest control on differences in light limitation.

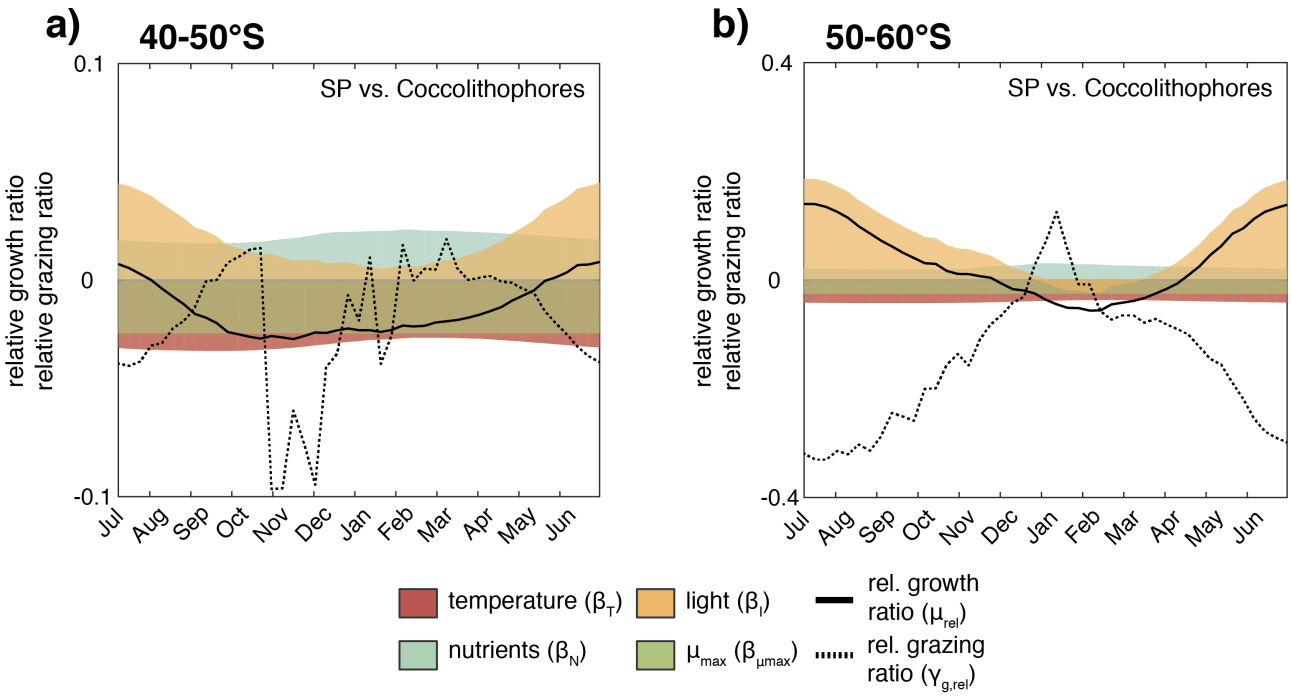

Figure S6: Relative growth ratio (solid black line) and relative grazing ratio (dashed black line) of small phytoplankton (SP) vs. coccolithophores for a) 40-50°S and b) 50-60°S. Colored areas are contributions of the maximum growth rate $\mu_{\max}$ (green), nutrient limitation (blue), light limitation (yellow) and temperature sensitivity (red) to the relative growth ratio, i.e. the red area e.g. represents the term β_{T} of Eq. 4 (see section 3 in main manuscript). Note that the scales in panel a) and b) are different.

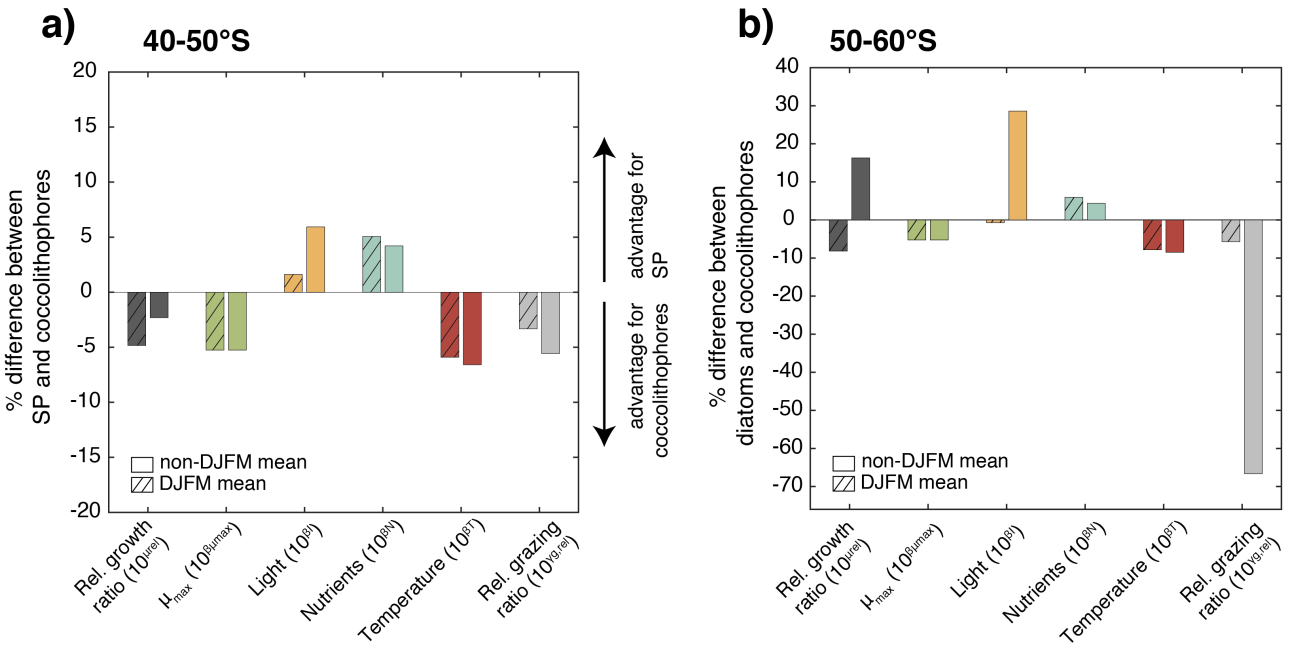

Figure S7: Percent difference in growth rate (dark grey), growth-limiting factors (maximum growth rate $\mu_{\max}$ in green, nutrient limitation in blue, light limitation in yellow and temperature sensitivity in red) and grazing rate (light grey) of small phytoplankton (SP) and coccolithophores for a) 40-50°S and b) 50-60°S. Respective left bar shows the December-March average (DJFM) calculated from the non-log transformed ratios (i.e. the red bar e.g. represents 10^{β_T}, see Eq. 4 in main manuscript), the shaded right bars show the average for all other months (non-DJFM). Full seasonal cycle is shown in Fig. S6.

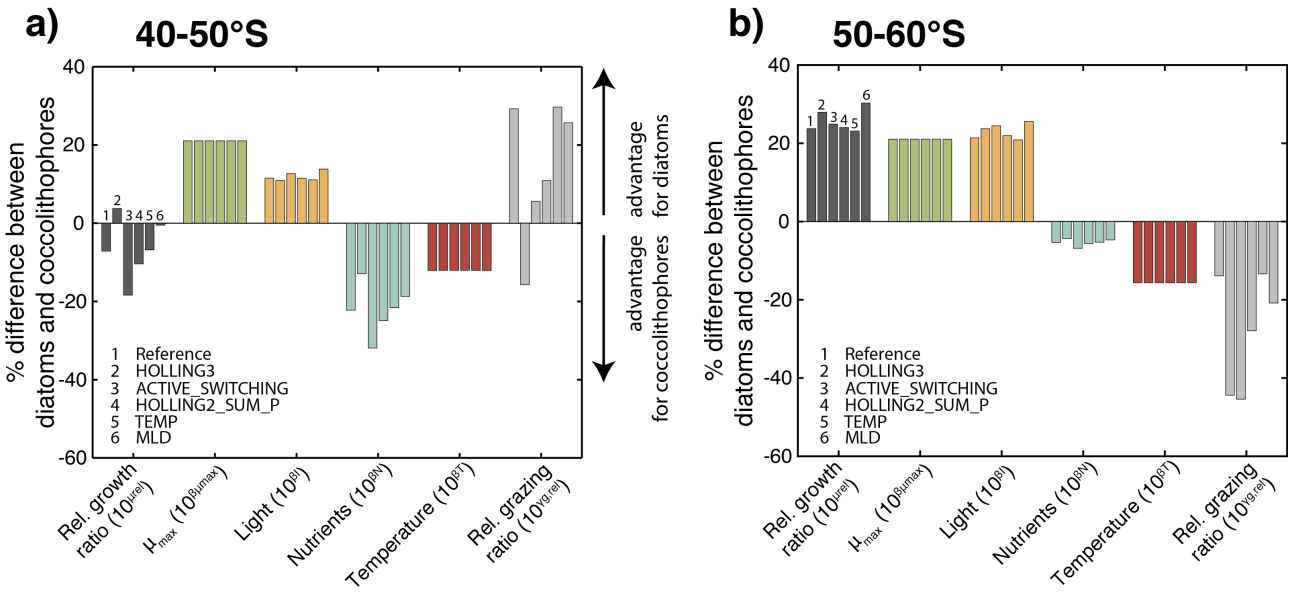

Figure S8: Assessing the effect of biases in the physical fields and the grazing formulation on the controlling factors of the relative importance of coccolithophores and diatoms: Annual mean percent difference in growth rate (dark grey), growth-limiting factors (maximum growth rate $\mu_{\max}$ in green, nutrient limitation in blue, light limitation in yellow and temperature sensitivity in red) and grazing rate (light grey) of diatoms and coccolithophores for a) 40-50°S and b) 50-60°S for the reference simulation (1), as well as HOLLINGIII (2), ACTIVE_SWITCHING (3), HOLLINGII_SUM_P (4), TEMP (5), and MLD (6) in Table 2 of the main text. Bars show the annual average calculated from the non-log transformed ratios (i.e. the red bar e.g. represents 10^{β_T}, see Eq. 4 in main manuscript).

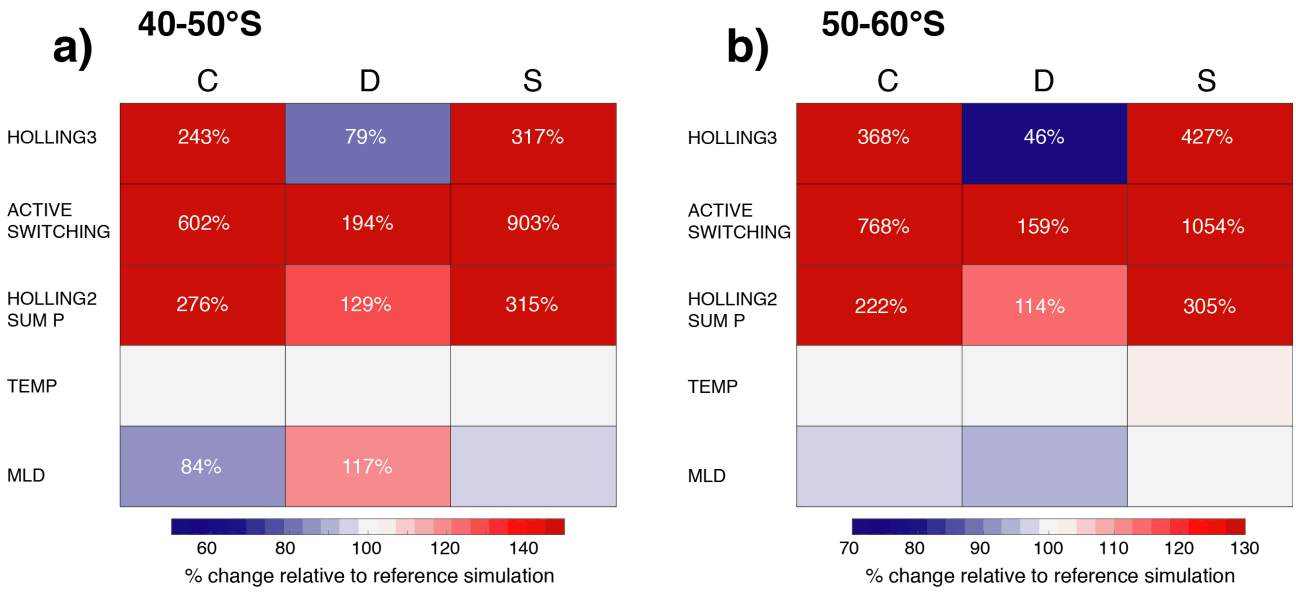

Figure S9: Relative change in annual mean surface chlorophyll biomass of coccolithophores, diatoms, and small phytoplankton (SP) for a) 40-50°S and b) 50-60°S for sensitivity simulations assessing grazing formulations and biases in the physical fields. See Table 2 in the main text for a description of the individual sensitivity simulations. Numbers of relative change are printed if change is larger than ±10%.

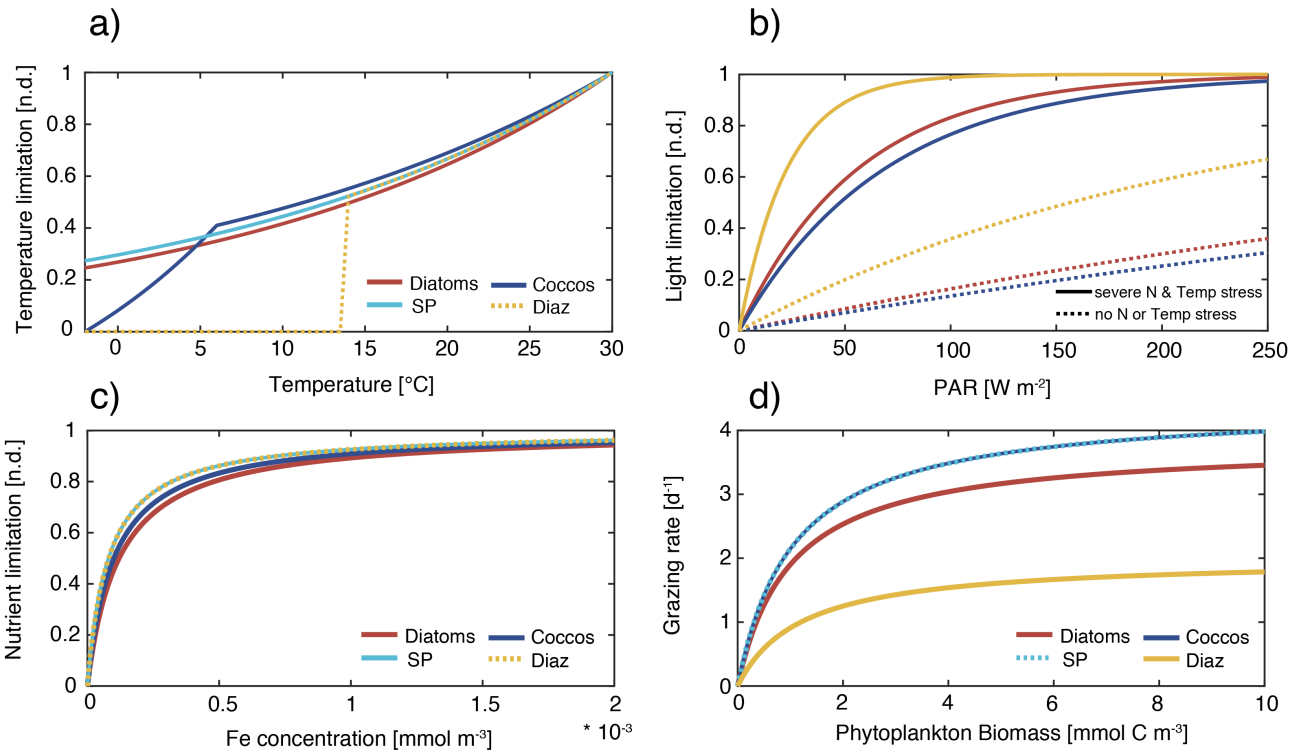

Figure S10: Functional responses used in ROMS-BEC for diatoms, coccolithophores, small phytoplankton, and diazotrophs: a) Temperature limitation (Eq. B5 in manuscript), b) light limitation (Eq. B9 in manuscript, using domain & annual mean surface chlorophyll-to-carbon ratio of each PFT and max. growth rate (dashed) or nutrient-temperature-limited growth rate (0.1·max. growth rate, solid), note that SP is not shown to enhance visibility as SP light limitation is very similar to that of diatoms (red), c) nutrient limitation (Eq. B6, example for iron shown here), and d) grazing rate on phytoplankton (note that the rate shown here will be further scaled with zooplankton biomass and the zooplankton temperature limitation in ROMS-BEC, see Eq. B12).

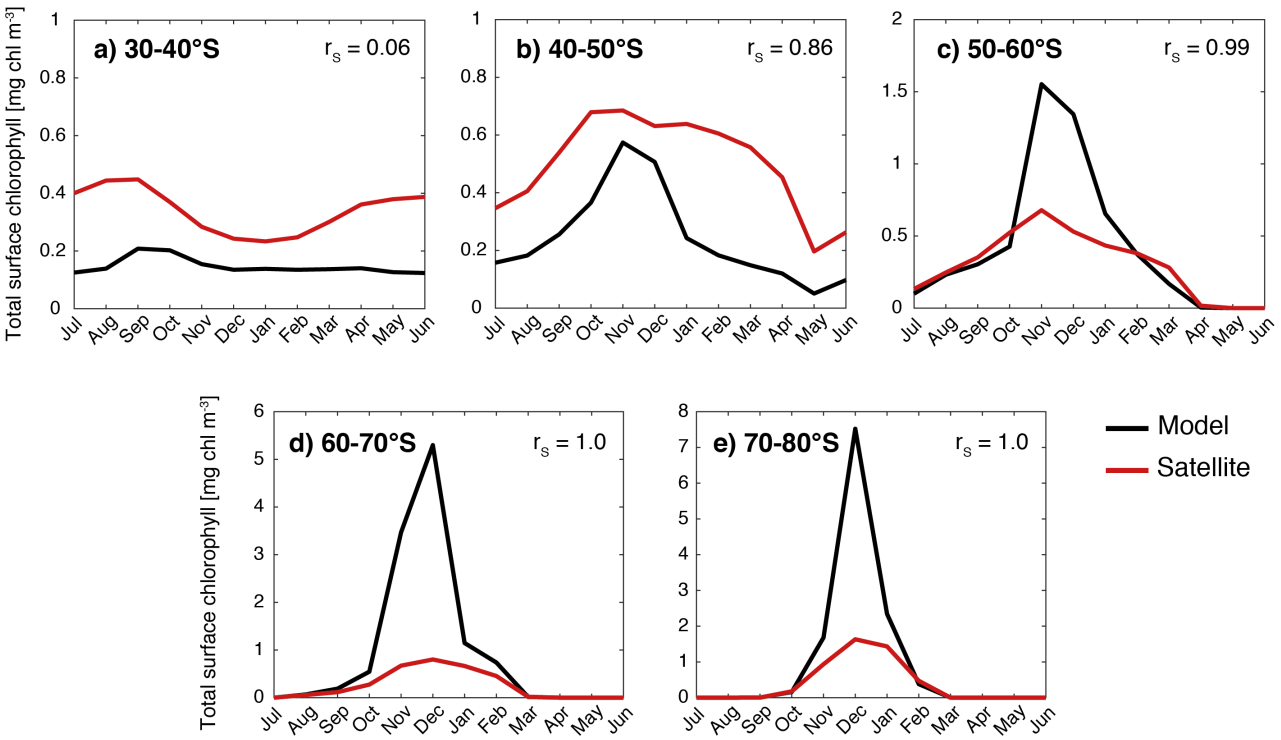

Figure S11: Surface total chlorophyll in the *Baseline* simulation of ROMS-BEC (black) as compared to satellite chlorophyll (red, MODIS-Aqua climatology) over the course of the year for a) 30-40°S, b) 40-50°S, c) 50-60°S, d) 60-70°S, and e) 70-80°S. Note the different scales in the panels. r_S in top right corner of each panel denotes the Spearman correlation coefficient.

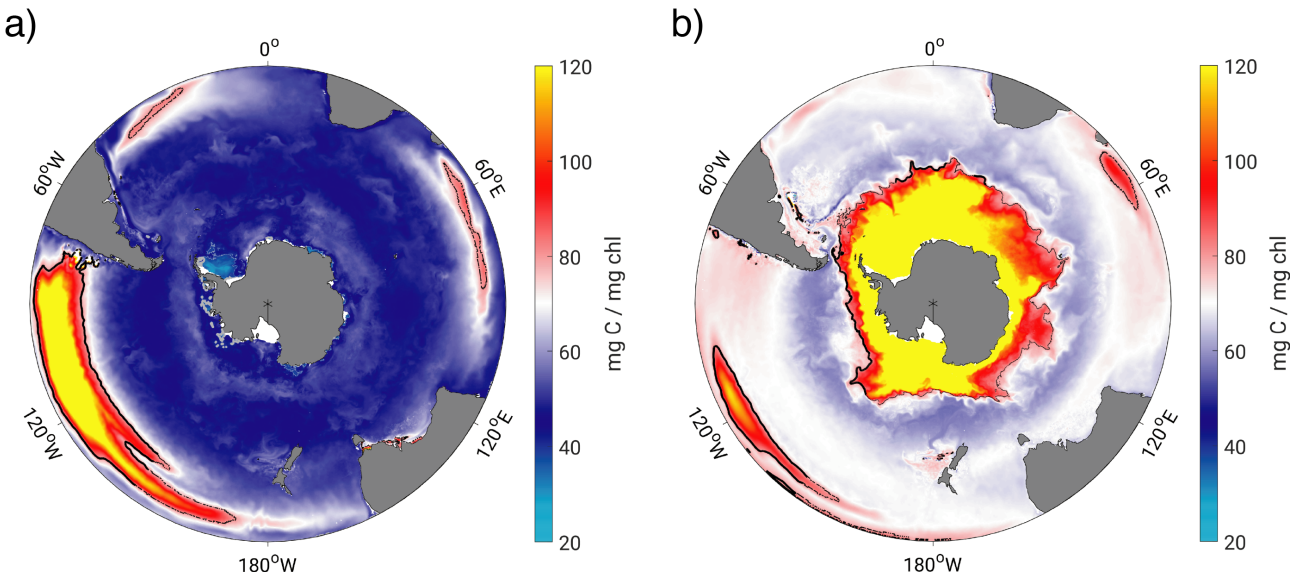

Figure S12: Annual mean surface carbon-to-chlorophyll ratios [mg C (mg chl)$^{-1}$] of a) diatoms and b) coccolithophores in the *Baseline* simulation of ROMS-BEC. The black contour corresponds to a ratio of 80 mg C (mg chl)$^{-1}$.

References

Balch, W. M., Drapeau, D., Bowler, B., and Booth, E.: Prediction of pelagic calcification rates using satellite measurements, Deep-Sea Res. Pt. II, 54, 478–495, https://doi.org/10.1016/j.dsr2.2006.12.006, 2007.

Balch, W. M., Bates, N. R., Lam, P. J., Twining, B. S., Rosengard, S. Z., Bowler, B. C., Drapeau, D. T., Garley, R., Lubelczyk, L. C., Mitchell, C., and Rauschenberg, S.: Factors regulating the Great Calcite Belt in the Southern Ocean and its biogeochemical significance, Global Biogeochem. Cy., pp. 1199–1214, https://doi.org/10.1002/2016GB005414, 2016.

Behrenfeld, M. J. and Falkowski, P. G.: Photosynthetic rates derived from satellite-based chlorophyll concentration, Limnol. Oceanogr., 42, 1–20, https://doi.org/10.4319/lo.1997.42.1.0001, 1997.

Cubillos, J. C., Wright, S. W., Nash, G., de Salas, M. F., Griffiths, B., Tilbrook, B., Poisson, A., and Hallegraeff, G. M.: Calcification morphotypes of the coccolithophorid Emiliania huxleyi in the Southern Ocean: changes in 2001 to 2006 compared to historical data, Mar. Ecol. Prog. Ser., 348, 47–54, https://doi.org/10.3354/meps07058, 2007.

Gravalosa, J. M., Flores, J.-A., Sierro, F. J., and Gersonde, R.: Sea surface distribution of coccolithophores in the eastern Pacific sector of the Southern Ocean (Bellingshausen and Amundsen Seas) during the late austral summer of 2001, Mar. Micropaleontol., 69, 16–25, https://doi.org/10.1016/j.marmicro.2007.11.006, 2008.

Leblanc, K., Arístegui, J., Armand, L., Assmy, P., Beker, B., Bode, A., Breton, E., Cornet, V., Gibson, J., Gosselin, M.-P., Kopczynska, E., Marshall, H., Peloquin, J., Piontkovski, S., Poulton, A. J., Quéguiner, B., Schiebel, R., Shipe, R., Stefels, J., van Leeuwe, M. A., Varela, M., Widdicombe, C., and Yallop, M.: A global diatom database abundance, biovolume and biomass in the world ocean, Earth Syst. Sci. Data, 4, 149–165, https://doi.org/10.5194/essd-4-149-2012, 2012.

Menden-Deuer, S. and Lessard, E. J.: Carbon to volume relationships for dinoflagellates, diatoms, and other protist plankton, Limnology and Oceanography, 45, 569–579, https://doi.org/10.4319/lo.2000.45.3.0569, 2000.

NASA-OBPG: NASA Goddard Space Flight Center, Ocean Ecology Laboratory, Ocean Biology Processing Group, Moderate-resolution Imaging Spectroradiometer (MODIS) Aqua Chlorophyll Data, https://doi.org/10.5067/AQUA/MODIS/L3M/CHL/2014, last accessed in Septemer 2016, 2014a.

NASA-OBPG: NASA Goddard Space Flight Center, Ocean Ecology Laboratory, Ocean Biology Processing Group, Moderate-resolution Imaging Spectroradiometer (MODIS) Aqua Particulate Inorganic Carbon Data, https://doi.org/10.5067/AQUA/MODIS/L3M/PIC/2014, last accessed in Septemer 2016, 2014b.

NASA-OBPG: NASA Goddard Space Flight Center, Ocean Ecology Laboratory, Ocean Biology Processing Group, Moderate-resolution Imaging Spectroradiometer (MODIS) Aqua Sea Surface Temperature Data, https://doi.org/missing, last accessed in Septemer 2016, 2014c.

O'Brien, C. J., Peloquin, J. A., Vogt, M., Heinle, M., Gruber, N., Ajani, P., Andruleit, H., Arístegui, J., Beaufort, L., Estrada, M., Karentz, D., Kopczyńska, E., Lee, R., Poulton, A. J., Pritchard, T., and Widdicombe, C.: Global marine plankton functional type biomass distributions: coccolithophores, Earth Syst. Sci. Data, 5, 259–276, https://doi.org/10.5194/essd-5-259-2013, 2013.

O'Malley, R.: Ocean Productivity website, data downloaded from http://www.science.oregonstate.edu/ocean.productivity/index.php, 2016.

Saavedra-Pellitero, M., Baumann, K.-H., Flores, J.-A., and Gersonde, R.: Biogeographic distribution of living coccolithophores in the Pacific sector of the Southern Ocean, Mar. Micropaleontol., 109, 1–20, https://doi.org/10.1016/j.marmicro.2014.03.003, 2014.

Smith, H. E. K., Poulton, A. J., Garley, R., Hopkins, J., Lubelczyk, L. C., Drapeau, D. T., Rauschenberg, S., Twining, B. S., Bates, N. R., and Balch, W. M.: The influence of environmental variability on the biogeography of coccolithophores and diatoms in the Great Calcite Belt, Biogeosciences, 14, 4905–4925, https://doi.org/10.5194/bg-14-4905-2017, 2017.

Soppa, M., Völker, C., and Bracher, A.: Diatom Phenology in the Southern Ocean: Mean Patterns, Trends and the Role of Climate Oscillations, Remote Sensing, 8, 420, https://doi.org/10.3390/rs8050420, 2016.

Swan, C. M., Vogt, M., Gruber, N., and Laufkötter, C.: A global seasonal surface ocean climatology of phytoplankton types based on CHEMTAX analysis of HPLC pigments, Deep-Sea Res. Pt. I, 109, 137–156, https://doi.org/10.1016/j.dsr.2015.12.002, 2016.

Tyrrell, T. and Charalampopoulou, A.: Coccolithophore size, abundance and calcification across Drake Passage (Southern Ocean), 2009, https://doi.org/10.1594/PANGAEA.771715, 2009.